

Journal of Materials Chemistry A

Accepted Manuscript



This is an *Accepted Manuscript*, which has been through the Royal Society of Chemistry peer review process and has been accepted for publication.

Accepted Manuscripts are published online shortly after acceptance, before technical editing, formatting and proof reading. Using this free service, authors can make their results available to the community, in citable form, before we publish the edited article. We will replace this *Accepted Manuscript* with the edited and formatted *Advance Article* as soon as it is available.

You can find more information about *Accepted Manuscripts* in the [Information for Authors](#).

Please note that technical editing may introduce minor changes to the text and/or graphics, which may alter content. The journal's standard [Terms & Conditions](#) and the [Ethical guidelines](#) still apply. In no event shall the Royal Society of Chemistry be held responsible for any errors or omissions in this *Accepted Manuscript* or any consequences arising from the use of any information it contains.

Hierarchical composites of TiO₂ nanowire arrays on reduced graphene oxide nanosheets with enhanced photocatalytic hydrogen evolution performance

Xinrui Cao,^a Guohui Tian,^{*a,b} Yajie Chen,^a Juan Zhou,^a Wei Zhou,^a Chungui Tian^a and Honggang Fu,^{*a}

Received (in XXX, XXX) Xth XXXXXXXXX 200X, Accepted Xth XXXXXXXXX 200X

First published on the web Xth XXXXXXXXX 200X

DOI: 10.1039/b000000x

In this study, hierarchical composites of reduced graphene oxide (RGO)-TiO₂ nanowire arrays were prepared via an in-situ controlled growth process and subsequent calcination. There formed a more homogeneous mixture and strong interaction between RGO nanosheets and anatase TiO₂ nanowires, which help the interfacial charge transfer and separation. Electrochemical impedance spectroscopy (EIS), surface photovoltage spectroscopy (SPV) and transient photovoltage (TPV) were used to study the interfacial charge transfer process. The prepared hierarchical RGO-TiO₂ nanowire array composites showed excellent H₂ production activity in the absence of noble metal cocatalysts, which was much higher than that of the pure anatase TiO₂ and RGO-TiO₂ generated by mechanically mixing. It was mainly attributed to the synergetic effect of the improved electron-hole pair separation rate, increased catalytic active sites and high light harvesting provided from the special hierarchical structure. The approach for the preparation of the hierarchical composite in this study may guide the way for designing new composite materials for enhanced photocatalytic and photoelectrochemical performance.

1. Introduction

Research progress nowadays has further showed that 1D nanostructures can be assembled into nanofibrous membranes to improve the photovoltage performance and self-cleaning ability.^{1,3} Especially, an array of highly ordered, vertically aligned 1D nanostructures have exhibited more excellent performance because the aligned nanostructure perpendicular to the substrate could potentially improve the charge-collection efficiency.¹⁴⁻¹⁷

As is well known, TiO₂ is one of most important semiconductor materials which was widely used in the field of photocatalysis.^{1,2} The photocatalytic performance of the TiO₂ is strongly dependent on its morphology and structure.³⁻⁵ Among the various morphologies, one dimensional (1D) TiO₂ nanomaterials such as nanowires and nanotubes, offering direct pathways for photogenerated electrons transfer, possess advantages such as facile charge transport along the longitudinal dimension, low electron-hole recombination rate, manifested superior photovoltaic and superhydrophilicity performance.⁶⁻⁹ Therefore, 1D TiO₂ has attracted extensive attention as a substitute for randomly oriented titania nanoparticles.¹⁰⁻¹² although among the various morphologies, 1D TiO₂ showed the better performance, pure 1D TiO₂ shows not satisfactory photocatalytic efficiency. Coupling TiO₂ with metal oxides, noble metal and other semiconductors is an effective approach to inhibit the electron-hole pair recombination and improve the photocatalytic activity.^{18,19}

Recently, reduced graphene oxide (RGO)-TiO₂ composites have shown advantageous enhancement of photocatalytic activity in a number of studies because the RGO can facilitate charge separation, possess high specific surface area, giant 2D

morphology and excellent electron conductivity.²⁰⁻²³ The present strategies to synthesize RGO-TiO₂ composites are usually directly depositing or simultaneously generating of TiO₂ with well defined structure (nanocrystallites or nanosheets) on GO sheets during the GO reduction. But the agglomeration of TiO₂ nanoparticles on RGO can prohibit the direct chemical contact between the two components. Therefore it will dramatically diminish photoelectron injection into RGO. This phenomenon may greatly reduce the synergetic catalytic effect of RGO and TiO₂ nanoparticles.^{24,25} In order to avoid this problem, 1D TiO₂ nanowires and nanotubes were reported to composite with graphene sheets, and showed enhanced charge separation and photocatalytic activity for the degradation of organic pollutants compared with the RGO-TiO₂ nanoparticles composites.²⁶ Although these results are promising, these 1D TiO₂ structures randomly deposit on the graphene in these composites. This composite pattern may reduce effective catalytic active sites and light utilization. Meanwhile, in comparison with the composites that 1D TiO₂ are in situ vertically growing on graphene, there may show weaker interaction between 1D TiO₂ and graphene, so influencing the further enhancement of photocatalytic activity. Recent study indicates the in situ controlled growth is capable of forming stronger interaction between two components with a tighter interface, which helps the interfacial charge transfer and reduces the self-agglomeration.²⁷ Furthermore, if 1D TiO₂ can grow closely on the graphene sheet substrate, the formed composite would serve as an ideal material for the H₂ production. However, to the best knowledge of the authors, there is no report on constructing hierarchical nanocomposites of the vertical 1D anatase TiO₂ nanowire arrays on graphene sheets.

Herein, we report a facile synthesis of hierarchical composites of reduced graphene oxide (RGO)-TiO₂ nanowire arrays and its performance in photocatalytic hydrogen evolution. The most notable aspect of our approach is that, the reduction of graphene oxide nanosheets and in situ vertical growth of TiO₂ nanowire arrays precursor on graphene oxide nanosheets are concurrent during solvothermal process. Finally, the RGO-precursor nanowire arrays composites were converted into RGO-anatase TiO₂ nanowire arrays composites after heat treatment, as illustrated in Scheme 1. In comparison with pure TiO₂ and RGO-TiO₂ generated by mechanically mixing, the enhanced photocatalytic hydrogen evolution performance of RGO-anatase TiO₂ nanowire arrays composites were generally attributed to the improved electron-hole pair separation and boosted catalytic active sites and light harvesting.

2. Experimental section

2.1. Synthesis of hierarchical composites of RGO-TiO₂ nanowire arrays

A certain amount of GO (prepared from natural graphite by a modified Hummers method²⁸) was dissolved into 25 mL of ethanol under stirring in order to be dispersed evenly, with a ratio of GO to TiO₂ (2, 3, 4 and 5 wt%). In the same typical case, 0.5 mL tetrabutyl titanate (TBOT) and 5 mL glycerol were added to the mixture, followed by stirring for another 5 minutes. The resulting solution was transferred into a 50 mL Teflon-lined stainless steel autoclave, which was heated to 180 °C and maintained for different time. Subsequently, the autoclave was cooled to room temperature naturally. The obtained solids were filtered, washed with ethanol and then dried at 60 °C. The as-prepared samples were calcined at 450 °C for 3 h under nitrogen protection. For comparison, bare RGO and pure TiO₂ were also obtained under the same experimental conditions. The mechanically mixed RGO-TiO₂ was prepared under the same experimental conditions by mixing GO with the TiO₂ nanowires.

2.2. Characterization.

The X-ray diffraction (XRD) of powder samples was examined by X-ray diffraction (XRD, Bruker D8 Advance diffractometer) monochromatized Cu K α radiation ($\lambda = 0.15418$ nm). Transmission electron microscopy (TEM) and high-resolution TEM (HRTEM) images of samples were recorded in a JEOL 2100 microscope with a 200 kV accelerating voltage, scanning electron microscopy (SEM, Hitachi, S-4800). Raman spectra were recorded on a Jobin Yvon HR 800 micro-Raman spectrometer at 457.9 nm. Surface area and pore size distribution for the samples were measured using a ASAP 2420 (Micrometrics Instruments) surface area analyzer that used the nitrogen adsorption-desorption method. The pore-size distribution (PSD) was obtained from the density functional theory (DFT) model in the Micromeritics ASAP2420 software package based on the N₂ sorption isotherm. The electrochemical impedance spectra (EIS) of the thin film made from these as-made materials were measured via a computer-controlled

IM6e impedance measurement unit (Zahner Elektrik, Germany) in 0.1 M Na₂S and 0.02 M Na₂SO₃ aqueous solution under UV light and carried out by applying sinusoidal perturbations of 10 mV under bias of -0.8 V, and the frequency ranges from 0.05 to 100 kHz. Transient photocurrent experiments were measured on an electrochemical analyzer (BAS100 Instruments) in a standard three-electrode system using the prepared samples as the working electrodes, a Pt wire as the counter electrode, and Ag/AgCl (saturated KCl) as a reference electrode. A low power UV-LED (3 W, 365 nm) was used as a light source, and 0.5 M Na₂SO₄ aqueous solution was employed as the electrolyte. Surface photovoltage spectroscopy (SPV) measurements of the samples were carried out with a home-built apparatus. The powder samples were sandwiched between two indium-tin oxide (ITO) glass electrodes, and the change of surface potential barrier between in the presence of light and in the dark was surface photovoltage signal. The raw SPV data were normalized with a Model Zolix UOM-1S illuminometer made in China. As for the transient photovoltage (TPV) measurement, the sample chamber consisted of an FTO electrode, a 10 mm thick mica spacer as electron isolator (to prevent the photoinduced electrons in the semiconductor from being directly injected to the electrode), and a platinum wire gauze electrode (with a transparency of about 50%). The construction was a sandwich like structure of FTO electrode/sample/mica/gauze platinum electrode, and the components of sandwich like structure were cascaded up directly by sequence without further treatment. During the measurement, the gauze platinum electrode was connected to the core of a BNC cable, which provided the input signals to the oscilloscope. The samples were excited from platinum wire gauze electrode with a laser radiation pulse (wavelength of 355 nm (50 mJ/cm²) and pulse width of 5 ns) from a thirdharmonic Nd:YAG laser (Polaris II, New Wave Research). The intensity of the pulse was determined with an EM500 singlechannel oulemeter (Molelectron). The TPV signals were registered with a 500 MHz digital phosphor oscilloscope (TDS 5054, Tektronix).

2.3. Measurement of photocatalytic hydrogen evolution.

The photocatalytic H₂ evolution from water was conducted in an online photocatalytic hydrogen production system (AuLight, Beijing, CEL - SPH2N). A powder sample of the catalyst (0.07 g) was suspended in a mixture of 100 mL of mixed aqueous solution containing 80 mL water and 20 mL methanol in a quartz reactor, without Pt co-catalyst. The reaction was carried out by irradiating the mixture with UV light from a 300 W Xe lamp with a 200-400 nm reflection filter which means the wavelength of light is approximately 200-400 nm. Prior to the reaction, the mixture was stirred to remove O₂ and CO₂ dissolved in water. Gas evolution was observed only under photoirradiation, being analyzed by an on-line gas chromatograph (SP7800, TCD, molecular sieve 5 Å, N₂ carrier, Beijing Keruida Limited).

3. Results and discussion

3.1. Characterization of phase structure and morphology.

The morphologies of the hierarchical composites of RGO-TiO₂ nanowires were characterized by SEM and TEM images and displayed in Fig. 1. As a comparison, the SEM image of the pure RGO obtained from solvothermal reaction is shown in Fig. 1A. RGO sheets are smooth with small wrinkles at the edges, and the height of the RGO nanosheets is about 5 nm, which corresponds to about 6 layers (Fig. S1). X-ray diffraction (XRD) patterns in Fig. 2A showed that the lattice plane of (001) at 10.5° (line a) of GO²⁹ disappeared (see line c) after the solvothermal reaction and calcination, indicating that the graphite oxide was exfoliated. The SEM and TEM images in Fig. S2 showed that the appearance of pure TiO₂ is flower-like aggregates composed of nanowires. For the hierarchical RGO-TiO₂ composite, the surface of each RGO nanosheet was covered with the uniform and upstanding anatase TiO₂ nanowires (Fig. 1B and Fig. S3), forming a hierarchical structure. From the image shown in Fig. 1D, it can be observed that calcination did not change the integral morphology of hierarchical structure compared with the initial uncalcined composite precursor (Fig. 1C). The structure of hierarchical composite was further examined by TEM and HRTEM. Fig. 1E shows the TEM image of an individual hierarchical RGO-TiO₂ composite. It is easy to find that the TiO₂ nanowires are adequately grown on the surface of RGO nanosheets, the average diameter and length of TiO₂ nanowires are about 10 nm and 400-600 nm, respectively. These TiO₂ nanowires are efficacious for electron transferring due to their one-dimension structure growing on the surface of RGO nanosheets. The corresponding high-resolution TEM (HRTEM) image (the magnification of the red square part of Fig. 1E) in Fig. 1F shows the fringe spacing of 0.35 nm corresponding well to that of the lattice space of (101) of anatase TiO₂,³⁰ which is consistent with the following XRD and Raman results in Fig. 2.

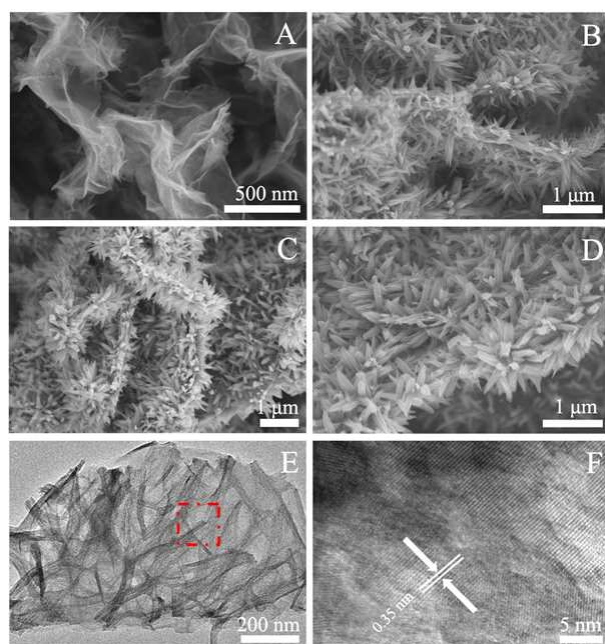


Fig. 1. SEM images of RGO (A), 3wt% RGO-TiO₂ composite (B and D) and 3wt% RGO-TiO₂ composite precursor (C); TEM (E) and HRTEM (F) images of the 3wt% RGO-TiO₂ composite.

Raman spectroscopy is a useful and powerful tool to characterize the crystalline quality in graphite materials. Fig. 2B shows the Raman spectra of GO, TiO₂ and hierarchical RGO-TiO₂ composite. Line a in Fig. 2B shows a Raman shift at 1368 and 1592 cm⁻¹ attributing to the D and G bands of GO, respectively.³¹ After solvothermal reaction, the positions of these bands had little change, and the G-band took on a characteristic asymmetric shape. Moreover, there is a slight increase of D/G ratio, with $I_D/I_G=0.79$ for graphene oxide versus $I_D/I_G=0.86$ for the RGO-TiO₂ nanocomposite, this change suggests the reduction of graphene oxide and the slight increase in the concentration of defects in this composite.³² While the peaks (Line c) centered at 157, 397, 518 and 643 cm⁻¹ were attributed to Raman modes of E_g(1), B_{1g}(1), A_{1g}(1)/B_{1g}(2) and E_g(2) of anatase TiO₂.³³ For the hierarchical RGO-TiO₂ composite, the intensity of these peaks corresponding to TiO₂ had a little decrease, which was due to the effect of RGO. The results further explained that nanowires were in situ grown on the surface of GO and GO was simultaneously reduced to RGO.³⁴

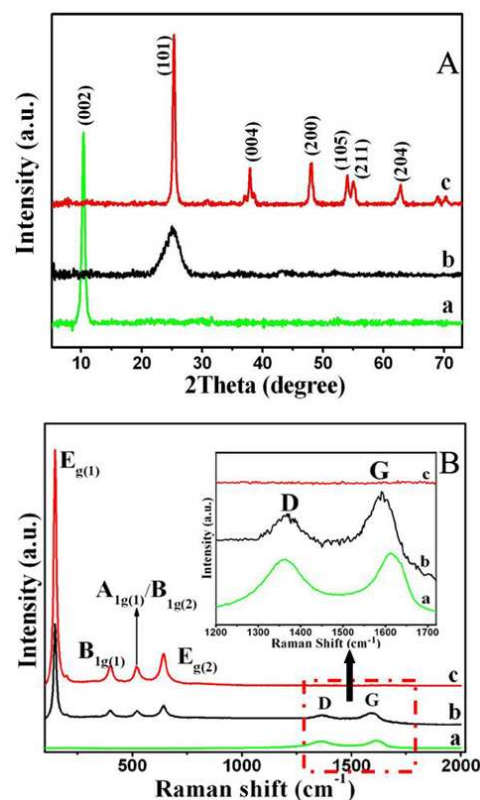


Fig. 2. XRD (A) and Raman (B) patterns of GO (a), 3wt% RGO-TiO₂ composite (b) and pure TiO₂ (c), respectively.

Fig. S4 shows the FTIR spectra of GO, TiO₂ and 3wt% RGO-TiO₂ composite. For the GO, oxygen functional groups such as, carboxylates C-O (1050 cm⁻¹), epoxide C-O-C (1230 cm⁻¹), and ketones (1700 cm⁻¹) can be found in the FTIR spectrum, and the absorption band appearing at about 1600 cm⁻¹ can be assigned to in-plane vibrations of aromatic C=C sp² hybridized carbons in GO.²⁶ For the 3wt% RGO-TiO₂ composite, the lack of oxygen features in the composite indicates the conversion of GO to RGO during solvothermal

treatment. The absorption peak (around 690 cm^{-1}) corresponding to Ti-O-Ti of TiO_2 shifted to higher wavenumber (798 cm^{-1}).^{26,35,36} The shift was attributed to the perturbation from RGO, confirming the presence of strong interaction between TiO_2 nanowires and RGO.^{26,35}

3.2. XPS spectra.

X-ray photoelectron spectroscopy (XPS) was used to confirm the formation of RGO from the reduction of GO through a solvothermal process. Fig. 3 shows the high-resolution XPS spectra of C1s region of GO and hierarchical RGO- TiO_2 composite. The two prominent peaks seen on the C1s XPS spectrum (Fig. 3A) of GO clearly indicated the presence of a considerable amount of oxygenated groups. The main C1s peak with a binding energy of 284 eV was assigned to adventitious carbon and sp^2 -hybridized carbon (C=C), and the sharp peak located at 286.6 eV was known to be hydroxyl carbon (C-O).^{36,37} As GO had higher degree of oxidation, the intensity of peak corresponding to hydroxyl carbon (C-O) was higher than sp^2 -hybridized carbon (C=C) (Fig. 3A). The peak at 288.2 eV corresponded to carboxyl carbon (O=C-O).³⁸ In comparison to the GO spectrum, the peak for O=C=O in the hierarchical RGO- TiO_2 composite (Fig. 3B) almost vanishes, and the peaks for C-O and C=C still exist but their intensities are much lower. The results reveal that GO was reduced to RGO under the effect of ethanol and glycerol during the solvothermal reaction, which is in good agreement with the Raman analysis. For the RGO- TiO_2 composite, two peaks (Fig. S5) at 458.6 and 464.5 eV assigned to the $\text{Ti}2\text{p}3/2$ and $\text{Ti}2\text{p}1/2$ in the Ti^{4+} chemical state, respectively, slightly shift toward higher binding energy compared to that of the pure TiO_2 .³⁹ This kind of shift in XPS measurement can be attributed to the presence of strong interaction at interfaces between titania and RGO. The intense interaction may result in the formation of electron transfer channel, which is beneficial to the improvement of photoinduced charge separation rate during the photocatalytic process.

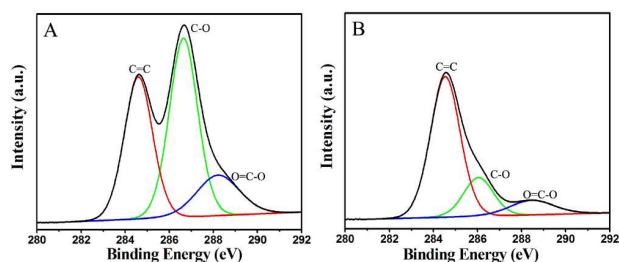


Fig. 3. High-resolution XPS spectra of C 1s for GO (A) and 3wt% RGO- TiO_2 (B).

3.3. Formation process of hierarchical structure precursor.

In order to study the morphological evolution of hierarchical structure precursor, time-dependent experiments were carried out. Products obtained at different growing stages were examined by SEM observation. As shown in Fig. 4A, there were only some nanoparticles growing on the surface of GO at the initial reaction stage (0.5 h). When the reaction time was prolonged to 1 h, these nanoparticles changed into small nanothorns (Fig. 4B). When the reaction

time was further extended to 4 h, the nanothorns got longer and uniformly dispersed on RGO (Fig. 4C). Finally, aligned nanowires arrays were covered on the surface of RGO nanosheets, and hierarchical structure composite formed after the reaction was carried out to 8 h (Fig. 4D). XRD patterns of products synthesized from different solvothermal reaction time are also shown in Fig. 5A. When the reaction time is only 0.5 h, there exists only diffraction peak (10.5°) corresponding to GO (line a in Fig. 5A). As the reaction time was prolonged, the diffraction peak corresponding to GO gradually disappeared, indicating the gradual reduction of GO. Meanwhile, the peaks corresponding to titanium glycerolate (TiGly) began to form when the reaction time reached 4 h. As the reaction time was further prolonged to 8 h, all diffraction peaks became stronger, indicating the structure development and complete formation of titanium glycerolate (TiGly) phase.⁴⁰ The results of XRD patterns in Fig. 5B confirmed that all the precursors changed to anatase TiO_2 (JCPDS No. 21-1272) after calcination.

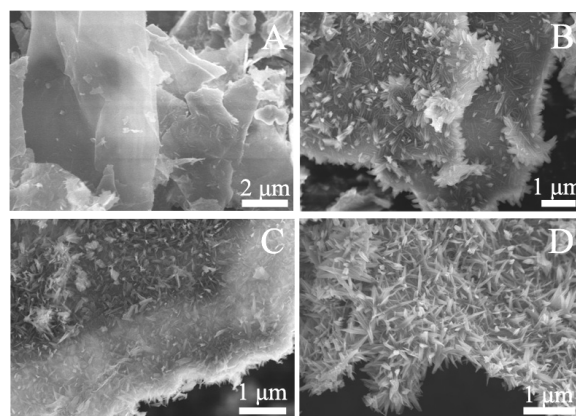


Fig. 4. SEM images of the obtained precursors prepared from different solvothermal reaction time: 0.5 h (A), 1 h (B), 4 h (C), 8 h (D).

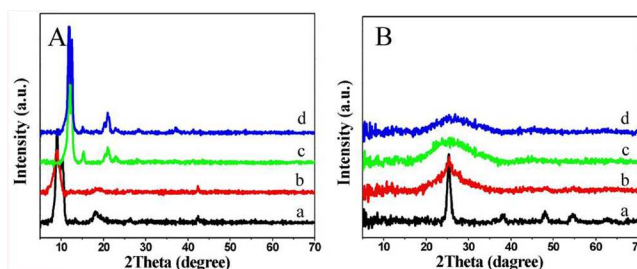
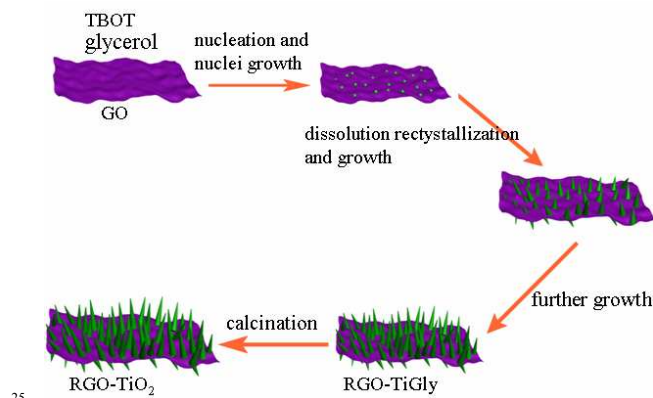


Fig. 5. XRD patterns of the prepared precursors (A) obtained from different solvothermal reaction time: 0.5 h (a), 1 h (b), 4 h (c), 8 h (d), and corresponding products after calcination (B).

3.4. Formation mechanism of hierarchical structure composites.

Based on the above experimental results and analysis, we proposed the formation mechanism (illustrated in Scheme 1) of hierarchical RGO- TiO_2 composite as follows: (i) fast nucleation and nuclei growth on GO nanosheets; (ii) dissolution-recrystallization growth; (iii) further growth, and subsequent calcination. In the formation process, hydrolysis and alcoholysis reactions of the tetrabutyl titanate can happen

at the initial reaction stage because of the existence of ethanol and a small amount of water produced from the release of etherifying reaction between ethanol and glycerol during solvothermal. As is known, there are various oxygen functional groups (e.g., hydroxyl, epoxy, and carbonyl groups) on the basal planes and edges of the 2D GO nanosheets.³² These functional groups can act as anchor sites and enable the formed amorphous titanium oxyhydrate nanoparticles in situ anchoring on the surfaces and edges of GO nanosheets by forming a Ti–O–C bond with GO.²⁶ With the increase of reaction time, the amorphous titanium oxyhydrate nanoparticles could change to titanium glycerolate (TiGly) complexes in the glycerol/ethanol reaction system. Similar to the previous report that the reaction between polyalcohol with metal ion usually form 1D coordination complexes,³⁹ in this experiment, the TiGly complexes would gradually grow along the initial nuclei of TiGly complexes and form long nanowire arrays (Fig. 4C,D) perpendicular to the 2D GO substrate due to the confinement effect of the GO. Moreover, in this process, GO was simultaneously reduced at high pressure and high temperature in the presence of glycerol and ethanol.³² So the hierarchical RGO-TiGly composite formed and then changed into hierarchical RGO-TiO₂ composite without integral morphology change after calcination.



Scheme 1 Illustration of the morphological evolution process of the hierarchical RGO-TiO₂ composite.

3.5. BET surface areas and pore size distributions.

The nitrogen adsorption-desorption isotherms and pore size distribution curves of different hierarchical RGO-TiO₂ composites are shown in Fig. S6. It can be seen that, compared with the pure TiO₂ (28 m² g⁻¹) as the contents of RGO increased, the Brunauer-Emmett-Teller (BET) surface areas of the samples of 2 wt% RGO-TiO₂, 3 wt% RGO-TiO₂, 4 wt% RGO-TiO₂ and 5 wt% RGO-TiO₂ showed an gradual increase from 31 m² g⁻¹, 56 m² g⁻¹, 78 m² g⁻¹ to be 104 m² g⁻¹, respectively. It is due to the gradual increase of the content of RGO with large surface area.^{41,42} The pore-size distribution (PSD) was obtained from the density functional theory (DFT) model in the Micromeritics ASAP2420 software package based on the N₂ sorption isotherm. The pore size distributions (Fig. S6B) results indicated the existence of aggregate pore structures resulting from microspaces surrounded by nanocrystals and the uneven surface structure of nanocrystals.

3.6. Photocatalytic activity.

The photocatalytic hydrogen production activities of aforementioned samples were measured. The changes of the amount of hydrogen evolution under the irradiation of UV light for different samples are shown in Fig. 6. Pure TiO₂ shows relatively low ultraviolet light photocatalytic H₂ production (7.86 μmol h⁻¹). However, in the presence of RGO, the RGO-TiO₂ composites exhibit obviously enhanced photocatalytic hydrogen production performance. The enhancement of hydrogen evolution could be attributed to the introduction of RGO with large surface area and excellent electronic conductivity,⁴³ which can promote the photogenerated electrons transport to the surface of the composite more easily, inhibiting the recombination between photogenerated electrons and holes.⁴⁴ Furthermore, in the composite, the introduction of RGO with high surface area can increase the amount of active sites.⁴⁵ The photocatalytic activity is maximized at the optimal RGO content in the catalyst. When the GO content reaches 3%, the catalyst 3wt% RGO-TiO₂ shows the best catalytic activity, the amount of hydrogen evolution enhanced with a rate of 20.12 μmol h⁻¹, which is 2.5 times higher than that of pure TiO₂ (7.86 μmol h⁻¹). The photocatalytic activity would decrease when GO content is further increased. It is because that some active sites of TiO₂ are disadvantageously occupied by the excess RGO. This leads to a decrease in the number of the active sites of the catalyst, resulting in the decrease of photocatalytic activity.⁴⁶ In addition, the content of RGO had a significant effect on the absorbing photons. With an increase in the content of RGO, the photons absorbed by the photocatalysts would reach a maximum. Then, the photons cannot be continuously injected into photocatalysts, which leads to excess recombination of electrons and holes.⁴⁷ These competing factors are compromised with each other upon 3wt% loading of RGO, at which the screening of active sites counterbalances the effect of increased surface area. Therefore, the composite of 3wt% RGO-TiO₂ shows the best photocatalytic activity.

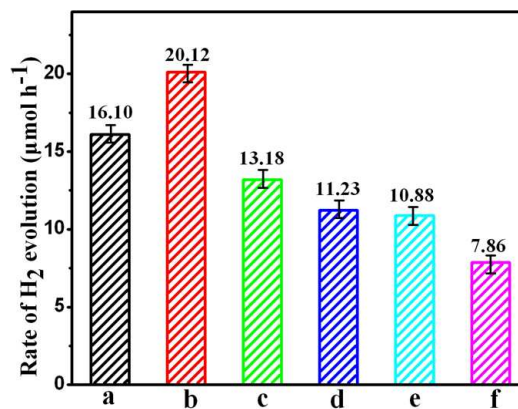


Fig. 6. Effect of RGO-TiO₂ molar ratio in the composites on the photocatalytic H₂ evolution rates under UV light illumination: 2 wt% RGO-TiO₂ (a), 3 wt% RGO-TiO₂ (b), 4 wt% RGO-TiO₂ (c), 5 wt% RGO-TiO₂ (d), 3 wt% RGO-TiO₂ generated by mechanically mixing (e) and pure TiO₂ (f). Catalyst amount is 0.07 g.

In order to prove the effects of the strong interaction between TiO₂ nanowires and RGO nanosheets on the photocatalytic activity, for comparison, the 3wt% RGO-TiO₂ generated by mechanically mixing was also prepared and the photocatalytic activity was measured. Its photocatalytic activity was much lower

than the hierarchical RGO-TiO₂ composite. It is mainly attributed to the fact that there exists close interfacial contact and strong interaction between TiO₂ nanowires and RGO nanosheets in the hierarchical RGO-TiO₂ composite. The growth orientation of one-dimension nanowires orientation on the surface of two-dimension RGO nanosheets plays an important role in the enhancement of photocatalytic activity. The synergetic catalytic effect of special hierarchical structure and strong interaction between RGO and anatase TiO₂ can provide improved electron-hole pair separation and boosted catalytic active sites and light harvesting.^{47,48} When RGO is coupled with TiO₂ nanowires, the photo-generated electrons can be easily transferred to the RGO moiety, leading to the efficient separation and prolonged recombination time of electron-hole pairs. Meanwhile, the existing way of TiO₂ nanowires oriented on the surface of RGO can avoid the excess aggregate of TiO₂ nanowires, increase the reaction active sites and promote reactant adsorption.²⁷

Previous studies showed that the amount of photocatalysts had significant influence on the H₂ production.⁴⁹ Here we also investigated the dependence of the H₂ production on the amount of RGO-TiO₂ composite photocatalysts (Fig. 7). The H₂ production rate rapidly increases from 7.28 μmol h⁻¹ in the presence of 0.03 g of RGO-TiO₂ to the maximum rate of 20.12 μmol h⁻¹ in the presence of 0.07 g of RGO-TiO₂ and then decreases to 12.27 μmol h⁻¹ in the presence of 0.13 g RGO-TiO₂, which indicated that the concentration of catalysts had a significant effect on the absorbing photons. With an increase in the concentration of catalysts, the photons absorbed by the catalysts would reach a maximum. Then, the photons can not be continuously injected into catalyst, which leads to increased recombination of electrons and holes.⁴⁷ Besides excessive amount of catalyst in the aqueous solution shielding the incident light, thus preventing the generation of electrons from the catalyst below. As a result, the rate of hydrogen production decreases.

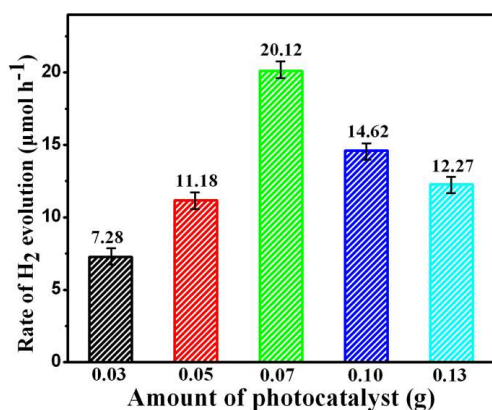


Fig. 7. Comparison of the photocatalytic H₂-production activity of 3wt% RGO-TiO₂ composite with different amounts.

It should be noted that, for a photocatalyst to be commercially viable, stability and high activity of the photocatalyst are both indispensable.⁵⁰ In order to investigate the photostability of hierarchical RGO-TiO₂ composite, the recycling experiments were also done. As shown in the Fig. S7, after four times consecutive recycling (12 h), the catalyst did not exhibit obvious loss of photocatalytic activity, indicating high stability of hierarchical RGO-TiO₂ composite

during photocatalytic H₂ production. Meanwhile, the property and structure of hierarchical RGO-TiO₂ composite was still stable. The XRD pattern and the SEM images (Fig. S8) of the hierarchical RGO-TiO₂ composite after four times consecutive recycling (12 h) of photoreaction are essentially similar to that of the original one, and there is no obvious deviation in the locations of these peaks, and the morphology also has no change, indicating that the hierarchical RGO-TiO₂ composite has considerable photostability.

We further compared the rates of H₂ evolution using ethylene diamine tetraacetic acid (EDTA) as electron donor instead of methanol. The results of the amount of hydrogen evolution are shown in Fig. S9. The similar result was observed for these samples, and the 3wt% RGO-TiO₂ sample still showed the best H₂ evolution performance. The above result revealed that CH₃OH is a better sacrificial agent for H₂ evolution than EDTA.

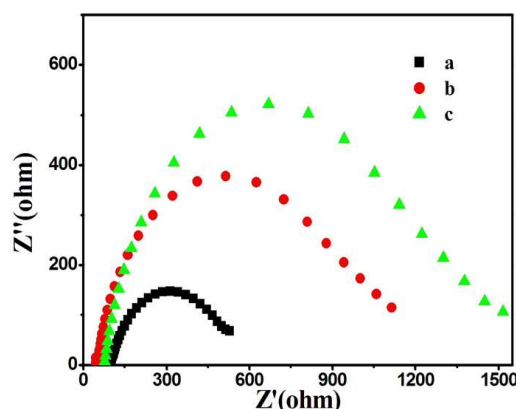


Fig. 8. EIS spectra of different samples: hierarchical 3wt% RGO-TiO₂ composite (a), 3wt% RGO-TiO₂ generated by mechanically mixing (b), and TiO₂ (c).

3.7. Charge transfer properties.

Recent years, electrochemical impedance spectroscopy (EIS) analysis has become a powerful tool in studying the charge transfer process occurring in the three-electrode system.³⁵ Since photocatalytic activity is directly related to the charge transfer and recombination rates, the solution-based electrochemical impedance spectroscopy (EIS) analysis data can further support the above conclusion. The EIS Nyquist plots of the different samples are shown in Fig. 8. The high frequency response is due to the charge transfer (or electrochemical reaction) at the Pt counter electrode, while the intermediate-frequency response is associated with the electron transport and transfer at the hierarchical RGO-TiO₂/electrode interface.⁵¹ The hierarchical RGO-TiO₂ composite shows the smallest semicircle in the middle-frequency region in comparison to the TiO₂ and RGO-TiO₂ generated by mechanically mixing, which indicates the fastest interfacial electron transfer.^{52,53} The results come from the combined effects. 1D TiO₂ nanowires and 2D RGO nanosheets can both benefit the charge transfer. Meanwhile, in the hierarchical RGO-TiO₂ system, the more homogeneous mixture and stronger interaction between two components with a tighter interface strong interaction can accelerate charge transfer and separation. Thus the photocatalytic H₂-production activity was significantly enhanced.

Transient photocurrent experiments were also done to study the charge transport between RGO and TiO₂. Fig. S10 shows a comparison of the transient photocurrent–time (*I*–*t*) curves for the above three samples with typical on–off cycles of intermittent visible light irradiation. Obviously, an apparently boosted photocurrent response appears for the three electrode samples under UV light illumination, and the on–off cycles of the photocurrent are reproducible. It can be found that the hierarchical 3 wt% RGO–TiO₂ composite showed the highest photocurrent value (88 μA cm⁻²). The magnitude of the photocurrent represents the charge collection efficiency of the electrode surface. This indicates that the hierarchical 3 wt% RGO–TiO₂ composite shows improved photogeneration of electrons and fast injection from TiO₂ into RGO, contributing to charge separation.

The surface photovoltage spectroscopy (SPV) is an effective technique to study the photophysics of excited states generated by photon absorption, and can effectively reflect the information about the separation and recombination of photoinduced charge carriers.⁵⁴ Fig. 9A shows the SPS spectra of the different samples. It can be seen that an obvious surface photovoltage response occurs at 300–400 nm. It can be related to the electron transitions from the valence band to the conduction band of TiO₂.⁵⁴ It can be seen that photovoltaic response of hierarchical RGO–TiO₂ composite is significantly higher than that of TiO₂, RGO–TiO₂ generated by mechanically mixing. Based on the results above, it can be concluded that, for the hierarchical RGO–TiO₂ composite prepared from the in situ growth, there exists more stronger interaction between TiO₂ and RGO, which makes the electron-hole pairs generating in the excited TiO₂ efficiently separated, resulting in the improving photovoltaic response of the hierarchical RGO–TiO₂ composite. We also used transient photovoltage (TPV) technique, an effective method for the investigation of dynamic properties of the photoinduced charge carriers in semiconductor materials,⁵⁵ to study the photovoltaic properties of as-synthesized hierarchical RGO–TiO₂ composite. As shown in Fig. 9B, there was a very low photovoltaic response of pure anatase TiO₂. However, it was interesting to find that after the integration of anatase TiO₂ nanowires with RGO nanosheets, its photovoltaic response showed significantly increase, which is 5 times higher than pure anatase TiO₂. It demonstrates that, after irradiation, the photo-induced electrons will transfer from anatase TiO₂ nanowires into RGO nanosheets, while the holes are left in anatase TiO₂ nanowires, which is proved by the positive signal of photovoltaic response, the electron-hole pairs generated in the excited anatase TiO₂ could be efficiently separated, resulting in the improved photovoltaic response of RGO–TiO₂ composite. However, the photovoltaic response of RGO–TiO₂ generated by mechanically mixing is much lower than the one produced by hierarchical RGO–TiO₂ composite, indicating that there exists more strong interaction between anatase TiO₂ nanowires and RGO nanosheets in the hierarchical RGO–TiO₂ composite. Meanwhile, it can also be seen that the mean life time of electron-hole pairs in the hierarchical RGO–TiO₂ composite is longer than the one of RGO–TiO₂ generated by mechanically mixing. It further

improved that the integration of RGO nanosheets with anatase TiO₂ nanowires by the approach of in situ growth would greatly retard the recombination electron-hole pairs in the excited anatase TiO₂ nanowires.

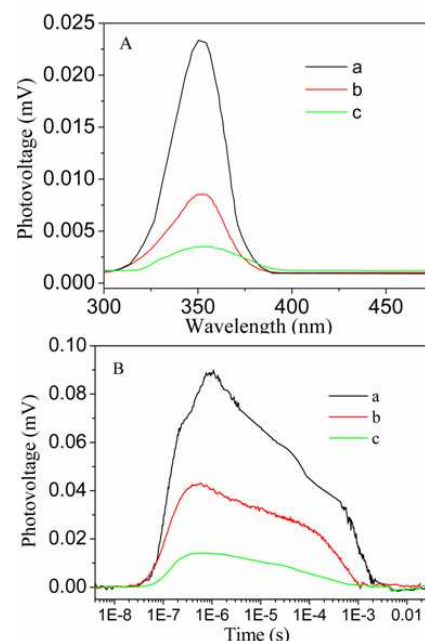


Fig. 9. Surface photovoltage spectroscopy (A) and transient photovoltage (TPV) responses (B) of different samples: hierarchical 3wt% RGO–TiO₂ composite (a), 3wt% RGO–TiO₂ generated by mechanically mixing (b), and TiO₂ (c).

4. Conclusions

In summary, hierarchical RGO–TiO₂ composites were prepared via an in situ controlled growth and subsequent calcination process with a high yield. In this process, TiO₂ nanowire arrays are delicately grown on 2D GO nanosheets. The morphology of TiO₂ nanowires can be controlled by adjusting the reaction time, which is attributed to different nucleation processes. There exists more strong interaction and interface contactation between anatase TiO₂ nanowires and RGO nanosheets in the hierarchical RGO–TiO₂ composites. The photocatalytic test results proved that, hierarchical RGO–TiO₂ composites showed much higher hydrogen evolution performance than the individual TiO₂ component and RGO–TiO₂ generated by mechanically mixing due to the synergistic effect of more catalytic active sites, improved charge separation and high light utilization. This work provides a facile approach to construct high photocatalytically active hierarchical structure composites using 1D and 2D nanocomponents with a high yield.

Acknowledgments

This research was supported by the National Natural Science Foundation of China (51272070, 21031001, 20971040, 21001042, 21101060, 21201058), the Cultivation Fund of the Key Scientific and Technical Innovation Project, Ministry of Education of China (No 708029), NSFC Projects of International Cooperation and Exchanges (51310105017),

Special Fund of Technological Innovation Talents in Harbin City (No. 2012RFQXG111), and the Scientific Research Fund of Heilongjiang Provincial Education Department (no. 11541283).

Notes

^a Key Laboratory of Functional Inorganic Material Chemistry, Ministry of Education of the People's Republic of China, Heilongjiang University, Harbin 150080 P. R. China

^b Key Laboratory of Chemical Engineering Process & Technology for High-efficiency Conversion, College of Heilongjiang Province, School of Chemistry and Materials Science, Heilongjiang University, Harbin 150080, China.

Corresponding author E-mail: tiangh@hlju.edu.cn; fuhg@vip.sina.com, Tel.: +86 451 8660 4330, Fax: +86 451 8667 3647

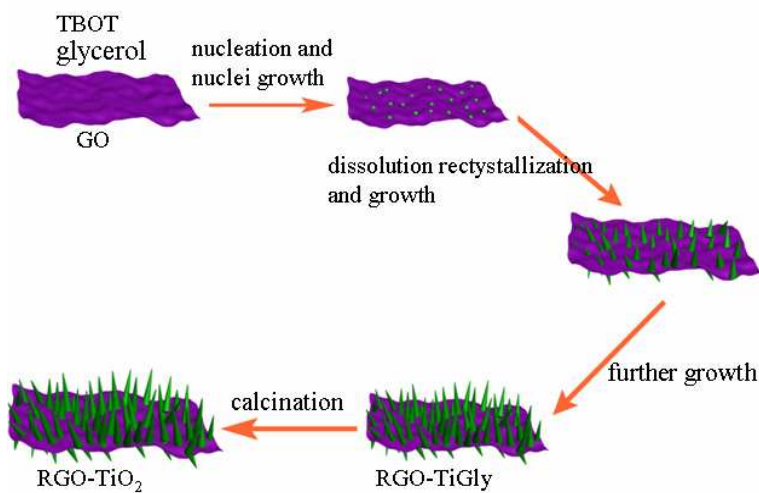
[†] Electronic Supplementary Information (ESI) available: [details of any supplementary information available should be included here. See DOI: 10.1039/b000000x/]

References

- H. B. Wu; H. H. Hong and X. W. Lou, *Adv. Mater.*, 2012, **24**, 2567.
- B. O'Regan and M. Grätzel, *Nature*, 1991, **353**, 737.
- W. X. Guo, C. Xu, X. Wang, S. H. Wang, C. F. Pan, C. J. Lin and Z. L. Wang, *J. Am. Chem. Soc.*, 2012, **134**, 4437.
- G. H. Tian, Y. J. Chen, H. L. Bao, X. Y. Meng, K. Pan, W. Zhou, C. G. Tian, J. Q. Wang and H. G. Fu, *J. Mater. Chem.*, 2012, **22**, 2081.
- M. Es-Souni, S. Habouti, N. Pfeiffer, A. Lahmar, M. Dietze and C. H. Solterbeck, *Adv. Funct. Mater.*, 2010, **20**, 377.
- M. Law, L. E. Greene, J. C. Johnson, R. Saykally and P. D. Yang, *Nat. Mater.*, 2005, **4**, 455.
- E. Galoppini, J. Rochford, H. H. Chen, G. Saraf, Y. C. Lu, A. Hagfeldt and G. Boschloo, *J. Phys. Chem. B*, 2006, **110**, 16159.
- D. J. Yang, H. W. Liu, Z. F. Zheng, Y. Yuan, J. C. Zhao, E. R. Waclawik, X. B. Ke and H. Y. Zhu, *J. Am. Chem. Soc.*, 2009, **131**, 17885.
- D. Kim, A. Ghicov, S. P. Albu and P. Schmuki, *J. Am. Chem. Soc.*, 2008, **130**, 16454.
- P. A. Sedach, T. J. Gordon, S. Y. Sayed, T. Furstenhaupt, R. H. Sui, T. Baumgartner and C. P. Berlinguette, *J. Mater. Chem.*, 2010, **20**, 5063.
- A. B. F. Martinson, J. E. McGarrath, M. O. K. Parpia and J. T. Hupp, *Phys. Chem. Chem. Phys.*, 2006, **8**, 4655.
- X. J. Feng, K. Shankar, O. K. Varghese, M. Paulose, T. J. Latempa and C. A. Grimes, *Nano Lett.*, 2008, **8**, 3781.
- P. Sudhagar, V. Gonzalez-Pedro, I. Mora-Sero, F. Fabregat-Santiago, J. Bisquert and Y. S. Kang, *J. Mater. Chem.*, 2012, **22**, 14228.
- B. Liu, A. Khare and E. S. Aydil, *Chem. Commun.*, 2012, **48**, 8565.
- B. Liu and E. S. Aydil, *J. Am. Chem. Soc.*, 2009, **131**, 3985.
- S. C. Hou, X. Cai, H. W. Wu, Z. B. Lv, D. Wang, Y. P. Fu and D. C. Zou, *J. Power Sources*, 2012, **215**, 164.
- K. Zhu, N. R. Neale, A. Miedaner and A. J. Frank, *Nano Lett.*, 2007, **7**, 69.
- (a) K. Dai, T. Y. Peng, D. N. Ke and B. Q. Wei, *Nanotechnology*, 2009, **20**, 125603. (b) J. Choi, N. King and Paul. A. Muggard, *ACS Nano*, 2013, **7**, 1699. (c) K. Dai, X. H. Zhang, K. Fan, T. Y. Peng and B. Q. Wei *Appl. Surf. Sci.*, 2013, **270**, 238.
- (a) K. Li, B. Chai, T. Y. Peng, J. Mao and L. Zan, *ACS Catal.*, 2013, **3**, 170. (b) K. Dai, T. Y. Peng, H. Chen, R. X. Zhang and Y. X. Zhang, *Environ. Sci. Technol.*, 2008, **42**, 1505. (c) C. W. Liu, H. B. Chen, K. Dai, A. F. Xue, H. Chen and Q. Y. Huang, *Mater. Res. Bull.*, 2013, **48**, 1499. (d) K. Dai, T. Y. Peng, H. Chen, J. Liu and L. Zan, *Environ. Sci. Technol.*, 2009, **43**, 1540.
- G. Williams, B. Seger and P. V. Kamat, *ACS Nano*, 2008, **2**, 1487.
- C. Chen, W. M. Cai, M. C. Long, B. X. Zhou, Y. H. Wu, D. Y. Wu and Y. J. Feng, *ACS Nano*, 2010, **4**, 6425.
- M. Q. Yang, N. Zhang and Y. J. Xu, *ACS Appl. Mater. Interfaces*, 2013, **5**, 1156.
- Y. H. Ng, I. V. Lightcap, K. Goodwin, M. Matsumura and P. V. Kamat, *J. Phys. Chem. Lett.*, 2010, **1**, 2222.
- D. H. Wang, D. Choi, J. Li, Z. G. Yang, Z. M. Nie, R. Kou, D. H. Hu, C. M. Wang, L. V. Saraf and J. G. Zhang, *ACS Nano*, 2009, **3**, 907.
- Y. Liang, H. Wang, H. S. Casalongue, Z. Chen and H. Dai, *Nano Res.*, 2010, **3**, 701.
- (a) S. D. Perera, R. G. Mariano, K. Vu, N. Nour, O. Seitz, Y. Chabal and K. J. Jr. Balkus, *ACS Catal.*, 2012, **2**, 949. (b) X. Pan, Y. Zhao, S. Liu, C. L. Korzeniewski, S. Wang and Z. Y. Fan, *ACS Appl. Mater. Interfaces*, 2012, **4**, 3944.
- (a) J. J. Xu, K. Wang, S. Z. Zu, B. H. Han and Z. X. Wei, *ACS Nano*, 2010, **4**, 5019. (b) L. F. He, R. G. Ma, N. Du, J. G. Ren, T. L. Wong, Y. Y. Li and S. T. Lee, *J. Mater. Chem.*, 2012, **22**, 19061.
- W. S. Hummers and R. E. Offeman, *J. Am. Chem. Soc.*, 1958, **80**, 1339.
- C. Nethravathia, B. Viswanathb, C. Shivakumarac, N. Mahadevaiah and M. Rajamathia, *Carbon*, 2008, **46**, 1773.
- G. H. Tian, K. Pan, Y. J. Chen, J. Zhou, X. H. Miao, W. Zhou, R. H. Wang and H. G. Fu, *J. Power Sources*, 2013, **238**, 350.
- Q. J. Xiang, J. G. Yu, W. G. Wang and M. Jaroniec, *Chem. Commun.*, 2011, **47**, 6906.
- J. Zhou, G. H. Tian, Y. J. Chen, X. Y. Meng, Y. H. Shi, X. R. Cao, K. Pan, and H. G. Fu, *Chem. Commun.*, 2013, **49**, 2237.
- (a) Q. J. Xiang, J. G. Yu and M. Jaroniec, *Nanoscale*, 2011, **3**, 3670. (b) F. Zhang, H. Q. Cao, D. M. Yue, J. X. Zhang and M. Z. Qu, *Inorg. Chem.*, 2012, **51**, 9544.
- X. Y. Zhang, H. P. Li, X. L. Cui and Y. H. Lin, *J. Mater. Chem.*, 2010, **20**, 2801.
- (a) H. Zhang, X. J. Lv, Y. M. Li, Y. Wang and J. H. Li, *ACS Nano*, 2010, **4**, 380. (b) Sakthive, S.; Kisch, H. *Angew. Chem. Int. Ed.* 2003, **42**, 4908.
- H. Li, S. Pang, S. Wu, X. Feng, K. McEullen and C. Bubeck, *J. Am. Chem. Soc.*, 2011, **133**, 9423.
- C. Zhu, S. Guo, P. Wang, L. Xing, Y. Fang, Y. Zhai and S. Dong, *Chem. Commun.*, 2010, **46**, 7148.
- X. Q. Wang, K. Naka, H. Itoh, S. Park and Y. Chujo, *Chem. Commun.*, 2002, **38**, 1300.
- B. Jiang, C. Tian, W. Zhou, J. Wang, Y. Xie, Q. Pan, Z. Ren, Y. Dong, D. Fu, J. Han and H. Fu, *Chem. - Eur. J.*, 2011, **17**, 8379.
- X. C. Jiang, Y. L. Wang, T. Herricks and Y. N. Xia, *J. Mater. Chem.*, 2004, **14**, 695.
- S. W. Liu, C. Liu, W. G. Wang, B. Cheng and J. G. Yu, *Nanoscale*, 2012, **4**, 3193.
- C. X. Xiang, M. Li, M. J. Zhi, A. Manivannan and N. Q. Wu, *J. Mater. Chem.*, 2012, **22**, 19161.
- A. K. Geim, *Science*, 2009, **324**, 1530.
- F. K. Meng, J. T. Li, Scott. K. C. Shing, M. J. Zhi and N. Q. Wu, *J. Am. Chem. Soc.*, 2013, **135**, 10286.
- (a) Md. S. A. S. Shah, A. R. Park, K. Zhang, J. H. Park and P. J. Yoo, *ACS Appl. Mater. Inter.*, 2012, **4**, 3893. (b) L. W. Zhang, H. B. Fu and Y. F. Zhu, *Adv. Funct. Mater.*, 2008, **18**, 2180.
- Q. J. Xiang, J. G. Yu and M. Jaroniec, *J. Am. Chem. Soc.*, 2012, **134**, 6575.
- Q. Li, B. D. Guo, J. G. Yu, J. R. Ran, B. H. Zhang, H. J. Yan and J. R. Gong, *J. Am. Chem. Soc.*, 2011, **133**, 10878.
- (a) L. Han, P. Wang and S. J. Dong, *Nanoscale*, 2012, **4**, 5814. (b) Y. H. Zhang, Z. R. Tang, X. Z. Fu and Y. J. Xu, *ACS Nano*, 2011, **5**, 7426.
- N. Z. Bao, L. M. Shen, T. Takata and K. Domen, *Chem. Mater.*, 2008, **20**, 110.
- K. Dai, Y. Yao, H. Liu, I. Mohamed, H. Chen and Q. Y. Huang, *J. Mole. Cata. A Chem.*, 2013, **374**, 111.
- N. L. Yang, Y. Y. Liu, H. Wen, Z. Y. Tang, H. J. Zhao, Y. L. Li and D. Wang, *ACS Nano*, 2013, **7**, 1504.
- X. Xin, X. F. Zhou, J. H. Wu, X. Y. Yao and Z. P. Liu, *ACS Nano*, 2012, **6**, 11035.
- (a) Y. H. Lin, D. J. Wang, Q. D. Zhao, M. Yang and Q. L. Zhang, *J. Phys. Chem. B*, 2004, **108**, 3202. (b) G. H. Tian, Y. J. Chen, R. T. Zhai, J. Zhou, W. Zhou, R. H. Wang, K. Pan, C. G. Tian and H. G. Fu, *J. Mater. Chem. A*, 2013, **1**, 6961.
- G. H. Tian, L. Q. Jing, H. G. Fu and C. G. Tian, *J. Hazard. Mater.*, 2009, **161**, 1122.

- 55 (a) P. Wang, T. Xie, H. Li, L. Peng, Y. Zhang, T. Wu, S. Pang, Y. Zhao and D. Wang, *Chem. Eur. J.*, 2009, **15**, 4366. (b) G. H. Tian, Y. J. Chen, X. Y. Meng, J. Zhou, W. Zhou, K. Pan, C. G. Tian, Z. Y. Ren and H. G. Fu, *ChemPlusChem*, 2013, **78**, 117. (c) P. Wang, Y. M. Zhai, D. J. Wang and S. J. Dong, *Nanoscale*, 2011, **3**, 1640.

Graphical Abstract



Hierarchical composites of reduced graphene oxide (RGO)-TiO₂ nanowire arrays were prepared via an in situ controlled growth process and subsequent calcination. The prepared hierarchical RGO-TiO₂ composites showed excellent H₂ production activity, which was much higher than that of the pure TiO₂ and RGO-TiO₂ generated by mechanically mixing.